ARTICLES

Preparation and Optical Properties of ThO_2 and Eu-Doped ThO_2 Nanotubes by the Sol−Gel Method Combined with Porous Anodic Aluminum Oxide Template

Zhi-Wei Lin, Qin Kuang, Wei Lian, Zhi-Yuan Jiang, Zhao-Xiong Xie,* Rong-Bin Huang, and Lan-Sun Zheng

State Key Laboratory for Physical Chemistry of Solid Surfaces and Department of Chemistry, College of Chemistry and Chemical Engineering, Xiamen University, Xiamen 361005, China

Received: April 3, 2006; In Final Form: August 24, 2006

In this paper, we report the synthesis of thorium oxide and Eu-doped thorium oxide nanotubes for the first time using the sol−gel method in porous anodic aluminum oxide template. Transmission electron microscopy, X-ray diffraction, and X-ray photoelectron spectroscopy were applied to characterize the morphology and structure of the as-prepared nanotubes. It has been demonstrated that Eu^{3+} ions were homogeneously doped into the ThO_2 crystal lattice. The optical properties resulting from Eu-doped products were investigated by means of photoluminescence spectroscopy. Strong visible light emissions were observed at low doping concentration, and the luminescent intensity decreased at high doping concentration. The luminescent centers were concluded to be the Eu^{3+} ions in the cubic (O_h) sites rather than the C_{3v} sites, which accounted well for the decrease of luminescent intensity at high doping concentration.

1. Introduction

Nanostructured materials have been intensively studied for the past decade because of their unique properties and the potential to tailor these properties toward specific applications.[1,2] Among the kinds of nanostructures, hollow nanostructures attract increasing attention due to potential applications in many areas such as small containers for encapsulation and host materials for loading catalysts, etc. With the development of nanoscience and nanotechnology, various synthetic techniques have been developed to prepare hollow nanostructured materials, including template-assisted methods and template-free methods.[3−6] Among these methods, the porous anodic aluminum oxide (AAO), a well-known hard template, plays an important role in the preparation of one-dimensional nanotubes and their arrays.[7−11] Meanwhile, sol−gel method has many unique advantages in the preparation of nanomaterials, such as high purity and easy to control synthesis procedures and components.[12−14] Herein, we combine the sol−gel and AAO template methods for a simple preparation of thorium dioxide (ThO_2) and Eu-doped ThO_2 nanotubes.

ThO_2 is a new and important material used in ceramics,[15] sensors,[16] catalysts,[17] and electrodes.[18,19] Although there are many studies on the separation and preparation of ThO_2 grains,[20−22] few papers have been concerned with the preparation and properties of nanostructured thorium oxide. Especially, synthesis of ThO_2 nanotubes or nanowires has not yet been reported to our knowledge. Furthermore, there has been an increasing interest in rare-earth (RE)-doped materials due to their potential application in photonics and optoelectronics.[23−25] In particular, the luminescence of Eu^{3+} is fascinating because the major emission band is centered near 612 nm, which is one of the three primary colors.[26] In this paper, we reported an AAO template-assisted sol−gel method to prepare high-yield ThO_2 nanotubes. Eu^{3+} ions were successfully doped into ThO_2 nanotubes by introducing Eu_2O_3 powder during the preparation process. The optical properties resulting from Eu-doping were investigated by means of the photoluminescence spectroscopy.

2. Experimental Section

The AAO templates were prepared using a one-step anodizing process as reported in our previous paper.[11] After preparation of the porous AAO film, the pores of AAO were widened to about 80 nm by dipping the AAO film into 5% phosphoric acid solution for a half-hour at room temperature. Then, the AAO template was rinsed with distilled water and kept in a desiccator under low pressure for more than 8 h in order to drive out the gases trapped inside the pores. The pore depth of the AAO templates was about 20 μm.

ThO_2 and Eu-doped nanotubes were synthesized via an AAO template-assisted sol−gel method. The thorium nitrate and europium oxide powder (totally about 1.0 g) with proper proportions (the atomic mole ratios between thorium and europium are about 1.0:0, 1.0:0.1, 1.0:0.3, 1.0:0.6, 1.0:1.0, and 1.0:1.2, respectively) were dissolved by adding nitric acid (60 wt %) in 50 mL of distilled water, and the resulting mixture was stirred in a water bath of 100 °C until a white sol was obtained. The pH value of the resulting sol is about 2−3. The AAO templates were immersed into the sol for 2 h under relative vacuum ambience. The AAO templates were then placed in a furnace and heated to 500 °C within 20 min. The AAO templates were kept at 500 °C for 2 h and then cooled to room temperature

* Corresponding author. Telephone: +86-592-2185667. Fax: +86-592-2183047. E-mail: zxxie@xmu.edu.cn.

10.1021/jp0620724 CCC: $33.50
Published on Web 10/12/2006

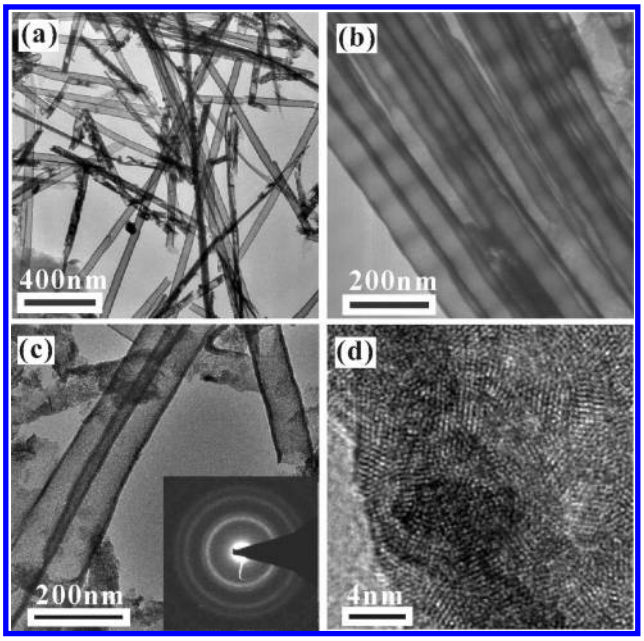

Figure 1. (a) Typical low-magnification TEM image of undoped ThO_2 nanotubes synthesized by sol−gel method in AAO templates. (b) Some bamboo-like nanotubes in the products. (c) Magnified TEM image of the undoped ThO_2 nanotubes. (d) HRTEM image of the wall of an individual undoped ThO_2 nanotube. The inset of c is a corresponding SAED image.

naturally. Excess products on the AAO surfaces were carefully wiped off. Before the analysis, the AAO templates were dissolved in enough amounts of NaOH (4 M) for more than 10 h to ensure the AAO template is totally dissolved. The final products were collected by centrifugalization and then rinsed with distilled water several times until the solution became neutral. As for the preparation of the samples for transmission electron microscopy (TEM) observations, the final products were first ultrasonically dispersed into ethanol solution and then deposited onto the copper grids.

The morphology and structure of final products were characterized by X-ray powder diffraction (XRD, Panalytical X-pert) using Cu Kα radiation, TEM (Hitachi H600), and high-resolution TEM (HRTEM, TECNAI F-30). The fluorescence spectra were measured by a photoluminescence spectrometer (F-4500) using a Xenon discharge lamp as the excitation light source, and the excited wavelength was 250 nm. The X-ray photoelectron spectroscopy (XPS) analyses were performed on a PHI quantum 2000 scanning ESCA microprobe equipped with an Al Kα monochromatic X-ray source.

3. Results and Discussion

3.1. Structure Characterization of ThO_2 and Eu-Doped ThO_2 Nanotubes. The AAO templates used in the experiment have an average pore diameter of 80 nm and a thickness of about 20 μm. Since previous reports showed that large quantities of alumina nanotubes/nanowires were obtainable by etching porous AAO templates in an aqueous NaOH solution at room temperature,[27] special attention should be paid not to mistake alumina nanotubes for the as-prepared nanotubes. To ensure all the aluminum oxide is dissolved, a high concentration of NaOH solution (4 M) was used to dissolve the corresponding AAO templates and the dissolving time was kept long enough (usually more than 10 h). Figure 1a shows a typical TEM image of as-prepared products without Eu^{3+}-doping. It can be seen that the final products consist of one-dimensional nanotubes.

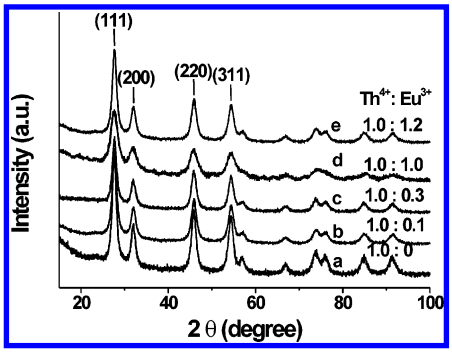

Figure 2. X-ray diffraction patterns of the as-prepared pure and Eu-doped ThO_2 nanotubes with different doping concentrations. The atomic mole ratios between Th^{4+} ions and Eu^{3+} ions are as follows: (a) 1.0:0 (pure ThO_2), (b) 1.0:0.1, (c) 1.0:0.3, (d) 1.0:1.0, and (e) 1.0:1.2, respectively.

The nanotubes are straight and have a uniform diameter of about 80 nm, which basically equals the pore size of the AAO template employed. The size and the morphology of the nanotubes do not change with the time for dissolving the AAO template, showing that the high concentration NaOH solutions do not affect the as-prepared nanotubes. It is also testified that the diameter of as-prepared nanotubes can be adjusted by choosing AAO templates with different pore size, indicating that the diameters of nanotubes are confined by the AAO pores during their growth. The lengths of these nanotubes are shorter than the pore depth of the AAO templates because the nanotubes are easily broken into short tubes during the ultrasonic dispersion process. At the same time, some bamboo-like nanotubes are observed in the product, as shown in Figure 2b. It is clearly found that the contrast of the nanotubes varied periodically along the long axes of the nanotubes. It should be pointed out that the morphologies have no obvious difference between undoped nanotubes and Eu^{3+}-doped samples with relatively low doping concentrations (such as the case in which the atomic mole proportion between thorium and europium is below 1.0:1.0). When the doping concentration was too high (for example, the atomic mole proportion between thorium and europium is 1.0:1.2), many irregular nanorods were observed.

Figure 1c is a magnified TEM image of the nanotubes, showing that the wall thickness of the nanotubes is about 8 nm. The selected area electron diffractions (SAED) of the nanotubes display a set of diffraction rings (see inset of Figure 1c), revealing that the nanotube is polycrystalline. According to the electron diffraction formula, the diffraction circles can be indexed as the diffractions from a cubic structure of thorium oxide. The HRTEM image taken from the wall of a nanotube confirms the polycrystalline nature of the nanotube, where the crystallite size is about 3−5 nm, as shown in Figure 1d. The lattice fringes in the HRTEM image are spaced 0.32 nm apart, which corresponds to the *d* value of (111) planes of the cubic thorium oxide (JCPDS No. 42-1462).

The typical XRD pattern of undoped ThO_2 nanotubes is shown in Figure 2a, in which all peaks are consistent with those of a cubic phase ThO_2 (JCPDS No. 42-1462). The relatively broadened diffraction peaks reveal that the nanotubes are composed of small nanoparticles. According to the Scherrer formula, the average diameter of the crystallites is estimated to be 4 nm. This result is in good agreement with the HRTEM observations.

It has been mentioned that the morphologies of the Eu-doped nanotubes have no obvious difference from that of the undoped ThO_2 nanotubes. To get deep insight into the structure of the Eu-doped nanotubes, the X-ray diffraction was carried out for

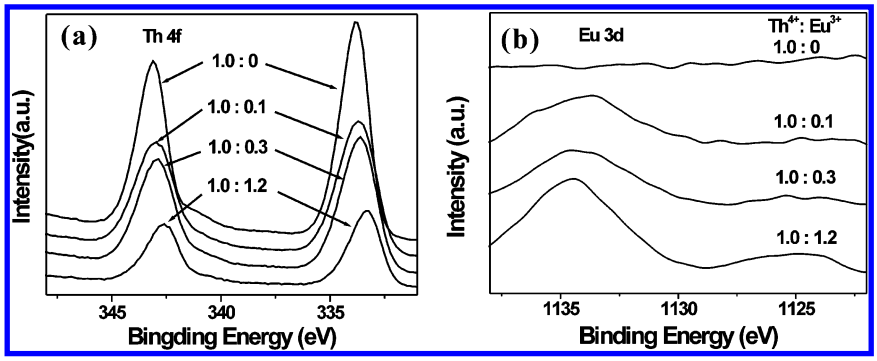

Figure 3. XPS spectra of (a) Th 4f and (b) Eu 3d as a function of Eu^{3+} concentration in Eu-doped ThO_2 nanotubes.

TABLE 1: Lattice Constants *a* (nm) of Eu-Doped ThO_2 Nanostructures

Th^{4+}:Eu^{3+}	*a* value (nm)	Th^{4+}:Eu^{3+}	*a* value (nm)
1.0:0	0.5596 ± 0.0001	1.0:1.0	0.5586 ± 0.0003
1.0:0.1	0.5595 ± 0.0002	1.0:1.2	0.5574 ± 0.0002
1.0:0.3	0.5591 ± 0.0002		

a serial of Eu^{3+}-doped ThO_2 samples with different doping concentrations (Figure 2b−e). It can be found that no additional crystal phase was observed after introducing Eu^{3+}, and all Eu-doped samples keep the same crystal phase as that of ThO_2. The results imply that the Eu^{3+} ions were homogeneously doped into the ThO_2 crystal lattice. Because the ionic radius of Eu^{3+} (0.095 nm) is smaller than that of Th^{4+} (0.104 nm), the replacement of Th^{4+} with Eu^{3+} results in the contraction of the crystal lattice. From the XRD patterns, the trend of the diffraction angles slightly shifting to high angle with the increase of the doping amount of Eu^{3+} is well-consistent with the hypothesis of lattice constant contraction after doping Eu^{3+}. Table 1 summarizes the crystal lattice parameters calculated from the XRD patterns for the Eu-doped products with different doping concentrations. The results show the decrease of crystal lattice parameters with the increase of Eu^{3+} concentration.

The doping of Eu^{3+} has further been checked by XPS, which is known to probe the elemental information of the surface of the materials. Parts a and b of Figure 3 respectively show the XPS spectra of the Th 4f region and the Eu 3d region of the ThO_2 nanotubes with different Eu^{3+} doping concentration. On the basis of the *Handbook of X-ray Photoelectron Spectroscopy*, we assign the peaks around 334.4 and 343.1 eV to the binding energies of Th 4f and the peak around 1134.0 eV to that of Eu 3d. It can be seen that the intensities of the Th 4f peaks decrease and those of Eu 3d increase with the increase of the Eu^{3+} concentration, confirming the successful doping of Eu^{3+}. Furthermore, with the increase of Eu-doping, the apexes of the Th 4f peaks shift to low binding energy, which could be due to replacement of the quadrivalence Th^{4+} by trivalence Eu^{3+}.

It is well-known that the sol−gel method is based on the hydrolysis and condensation of precursor solution such as organic metal alkoxides in organic solvents or inorganic salts in aqueous media. The biggest advantage of this sol−gel method is that the constituent materials can be easily homogeneously mixed at the molecular level by means of properly controlling the hydrolysis and condensation process. Therefore the sol−gel method can be an effective and versatile method for the preparation of homogeneous multicomponent materials. The successful doping of Eu^{3+} ions in the ThO_2 lattices at a wide doping concentration range in our experiments shows such a universality of the sol−gel method.

In recent years, the hard synthetic templates bring new opportunity for the preparation of one-dimensional (1D) mono-component and multicomponent nanostructures such as nanowires/nanotubes. Especially, porous AAO template plays an increasingly important role in the synthetic field of 1D nanostructures and their arrays due to its size-limiting effect and the high order of the pores. Combined with the sol−gel method, numerous monocomponent and multicomponent nanostructures have been successfully prepared by using porous AAO template.[10,12,28−32] However, most of the products are polycrystalline nanowires or the mixture of nanowires and nanotubes. The successful examples of high-yield and well-shaped nanotubes are seldom reported.[10,28,32] During the preparation of the sol in our experiment, we simply use metallic nitrate. Although the detail mechanism of the nanotube formation by our method is still unknown, the as-prepared gels could tend to heterogenerously adsorb and nucleate on active sites on the AAO pore walls and thus form a tubular structure. By means of the analogous method, we have also succeeded in obtaining a series of rare-earth metal oxide nanotubes from rare-earth metal nitrate recently. Therefore, our proposed porous AAO template assisted sol−gel method could be a versatile method and has potential application in the preparation of the polycrystalline nanotubes.

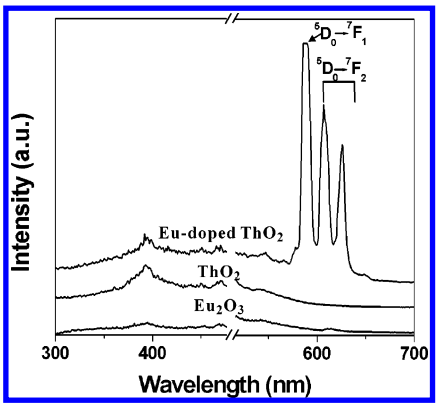

Figure 4. Fluorescence emission spectra of pure Eu_2O_3 powders, pure ThO_2 nanotubes, and Eu-doped ThO_2 nanotubes (atomic ratio of 1.0:0.1 between Th^{4+} and Eu^{3+} ions) at room temperature (λ_{ex} = 250 nm).

3.2. Optical Properties of ThO_2 and Eu-Doped ThO_2 Nanotubes. Figure 4 shows the room-temperature photoluminescence spectra from the original ThO_2 nanotubes, Eu_2O_3 powder, and Eu-doped ThO_2 nanotubes (atomic ratio of 1.0:0.1 between Th^{4+} and Eu^{3+} ions) under excitation at 250 nm, respectively. We divide the spectra into 300−480 nm (left) and 530−700 nm (right), as a very high second-order line appears at about 500 nm. It can be seen that there is no strong emission peak in the wave range of visible light for the pure ThO_2 nanotubes and the Eu_2O_3 powder. However, the emission spectrum shows several very strong peaks located at 590, 610, and 626 nm for the Eu-doped nanotubes in the case of the atomic ratio of 1.0:0.1 between Th^{4+} and Eu^{3+} ions. Clearly, the

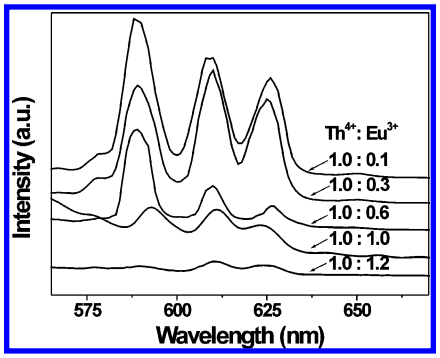

Figure 5. Room-temperature fluorescence emission spectra as a function of Eu^{3+} concentration in Eu-doped ThO_2 nanotubes.

luminescence was due to the doping of Eu^{3+} ions in ThO_2. To study the doping effect on the luminescence, the photoluminescence of Eu^{3+}-doped ThO_2 with different doping concentrations was studied. Figure 5 shows the luminescence spectra with different doping concentrations. The luminescence intensities around 590, 610, and 626 nm do not change much in the atom ratio range of 1.0:0.1 to 1.0:0.6. However, these visible luminescence intensities decrease if doping concentration further increases.

ThO_2 adopts a fluorite structure, where oxygen atoms adopt simple cubic packing and the Th^{4+} ions possess half of the cubic interstices of oxygen. The Th^{4+} ions are cubically coordinated by oxygen ions, and they adopt the O_h symmetry. While Eu^{3+} ions were doped into ThO_2 crystallite, the Eu^{3+} ions replace the site of Th^{4+}. As the valence of Eu^{3+} ions is lower than that of Th^{4+} ions, it has been thought oxygen vacancies should be formed for the charge compensation after doping the Eu^{3+} ions, and the coordination polyhedra of Eu^{3+} ions then change from the O_h symmetry to the C_{3v} symmetry (one site of the cube becomes a vacancy). In fact, because only half of the oxygen cubic interstices are possessed in a normal fluorite structure, another half of the cubic interstices may be possessed by the doping Eu^{3+} ions to compensate for the charges. In this case, the coordination polyhedra of Eu^{3+} ions may still adopt the O_h symmetry. It is reasonable to suppose that Eu^{3+} ions are likely to adopt the O_h symmetry when the doping concentration is low. Only when the doping concentration is high, the Eu^{3+} ions with C_{3v} symmetry appear. Linares also came to such a conclusion that the doping ions predominantly occupy the cubic sites (O_h symmetry) at low doping concentration, while they occupy the C_{3v} site at high concentration.[33]

Lanthanides are useful materials in optoelectronic devices and displays. The luminescence center of Eu^{3+}-doped ThO_2 was thought to be Eu^{3+} ion sites and has been studied by several groups.[34,35] Since the doped Eu^{3+} ions used to be thought at the C_{3v} sites, earlier study assigned these luminescence centers to the Eu^{3+} ions at C_{3v} sites (the peak of 590 corresponds to the $^5D_0 \rightarrow {}^7F_1$ transition, and the peaks of 610 and 626 nm correspond to $^5D_0 \rightarrow {}^7F_2$).[29] If it is the case, the intensities of the three peaks should increase with the increase of doping concentration. Obviously, the experimental result contradicts the proposed luminescence centers. Recently, the crystal-field energy levels of Eu^{3+} ions in C_{3v} symmetry and O_h symmetry were reported in detail.[23] From the reported crystal-field energy levels, there are only one energy level for $^7F_1$ state (irreducible representation is T) and two energy sublevels for $^7F_2$ state (irreducible representations are T and E, respectively) when Eu^{3+} ions are in the O_h symmetry; but there are two energy sublevels for $^7F_1$ (irreducible representations are A_2 and E, respectively) and three energy sublevels for the $^7F_2$ state (irreducible representations are A_1, E, and E, respectively) when Eu^{3+} ions adopt the C_{3v} symmetry. Hence, there should be two peaks corresponding to the $^5D_0 \rightarrow {}^7F_1$ transition and three peaks to $^5D_0 \rightarrow {}^7F_2$ for C_{3v} symmetry, but only one peak corresponding to the $^5D_0 \rightarrow {}^7F_1$ transition and two peaks to $^5D_0 \rightarrow {}^7F_2$ for O_h symmetry. Our results are in good agreement with the later one, i.e., the strong luminescence centers to be Eu^{3+} ions in cubic (O_h) sites. At low concentration, the doped Eu^{3+} ions predominantly occupy the cubic sites (O_h symmetry), and the intensities of the luminescent peaks increase with the doping density. While the doping concentration further increases, the Eu^{3+} ions occupy the C_{3v} sites and the Eu^{3+} ions in cubic sites decrease. Therefore, these three strong luminescent peaks decrease at high doping concentration. In the pure Eu_2O_3 powder, there is no Eu^{3+} ion in cubic (O_h) sites, and thus the three emission lines cannot be observed.

4. Summary

In summary, both pure and Eu-doped ThO_2 nanotubes have been successfully fabricated by sol−gel method with the assistance of porous AAO templates. The Eu-doped ThO_2 nanotubes adopt the same cubic structure as that of ThO_2. The walls of the nanotubes are polycrystalline and their crystallite size is about 3−5 nm. Combining XRD and XPS measurements, we confirm the Eu^{3+} ion has been successfully doped into ThO_2. Photoluminescence properties of Eu-doped in ThO_2 nanotubes are also studied, which shows strong visible light emission occurs at low concentration doping, and the luminescent intensity decreases at high concentration doping. The Eu^{3+} ions in the cubic (O_h) sites are thought to be the luminescent center in the Eu-doped ThO_2 nanotubes, which can well account for the decrease of luminescent intensity at high doping concentration.

Acknowledgment. This work is supported by the NSFC (Grant Nos. 20673085 and 20473069), the NSF of Fujian Province (Grant No. E0310004), the Key Scientific Project of Fujian Province of China (Grant No. 2005HZ01-3), NCET and SRF for ROCS from the Ministry of Education of China, and the Fok Ying-Tung Educational Foundation.

References and Notes

(1) Wang, Z. L., Ed. *Nanowires and Nanobelts: Materials, Properties and Devices*; Tsinghua University Press: Beijing, 2004.
(2) Kuang, Q.; Jiang, Z. Y.; Xie, Z. X.; Lin, S. C.; Lin, Z. W.; Xie, S. Y.; Huang, R. B.; Zheng, L. S. *J. Am. Chem. Soc.* **2005**, *127*, 11777.
(3) Zelenski, C. M.; Dorhout, P. K. *J. Am. Chem. Soc.* **1998**, *120*, 734.
(4) Xia, Y.; Yang, P.; Sun, Y.; Wu, Y.; Mayers, B.; Gates, B.; Yin, Y.; Kim, F.; Yan, Y. *Adv. Mater.* **2003**, *15*, 353.
(5) Jiang, Z. Y.; Xie, Z. X.; Zhang, X. H.; Huang, R. B.; Zheng, L. S. *Chem. Phys. Lett.* **2003**, *378*, 313.
(6) Jiang, Z. Y.; Xie, Z. X.; Zhang, X. H.; Lin, S. C.; Xu, T.; Xie, S. Y.; Huang, R. B.; Zheng, L. S. *Adv. Mater.* **2004**, *16*, 904.
(7) Lee, J. S.; Gu, G. H.; Kim, H.; Jeong, K. S.; Bae, J.; Suh, J. S. *Chem. Mater.* **2001**, *13*, 2387.
(8) Peng, T. Y.; Yang, H. P.; Dai, K.; Pu, X. L.; Hirao, K. *Chem. Phys. Lett.* **2003**, *379*, 432.
(9) Tan, H.; Ye, E.; Fan, W. Y. *Adv. Mater.* **2006**, *18*, 619.
(10) Cheng, L. F.; Zhang, X. T.; Liu, B.; Wang, H. Z.; Li, Y. C.; Huang, Y. B.; Du, Z. L. *Nanotechnology* **2005**, *16*, 1341.
(11) Zhang, S. H.; Xie, Z. X.; Jiang, Z. Y.; Xu, X., Xiang, J.; Huang, R. B.; Zheng, L. S. *Chem. Commun.* **2004**, 1106.
(12) Xu, H.; Qin, D. H.; Yang, Z.; Li, H. L. *Mater. Chem. Phys.* **2003**, *80*, 524.
(13) Hernandez, B. A.; Chang, K. S.; Fisher, E. R.; Dorhout, P. K. *Chem. Mater.* **2002**, *14*, 480.
(14) Lin, Y.; Sun, F. Q.; Yuan, X. Y.; Geng, B. Y.; Zhang, L. D. *Appl. Phys. A: Mater. Sci. Process.* **2003**, *78*, 1197.

(15) Curran, G.; Sevestre, Y.; Rattray, W.; Allen, P.; Czerwinski, K. R. *J. Nucl. Mater.* **2003**, *323*, 41.

(16) Niranjan, R. S.; Londhe, M. S.; Mandale, A. B.; Sankar, S. R.; Prabhumirashi, L. S.; Vijayamohanan, K.; Mulla, I. S. *Sens. Actuators, B* **2002**, *87*, 406.

(17) Ho, S. W. *J. Catal.* **1998**, *175*, 139.

(18) Ge, F. Z.; Ye, Z. Z.; Wang, F. Z.; Wang, Y. P.; Zhang, H.; Ding, B. J. *Mater. Lett.* **2003**, *57*, 2776.

(19) Zhang, H.; Chen, X. F.; Yang, Z. M.; Ding, B. *J. Mater. Lett.* **1999**, *38*, 401.

(20) Li, D. Q.; Zuo, Y.; Meng, S. L. *J. Alloys Compd.* **2004**, *374*, 431.

(21) Reibold, R. A.; Poco, J. F.; Baumann, T. F.; Simpson, R. L.; Satcher, J. H. *J. Non-Cryst. Solids* **2004**, *341*, 35.

(22) Dash, S.; Singh, A.; Ajikumar, P. K.; Subramanian, H.; Rajalakshmi, M.; Tyagi, A. K.; Arora, A. K.; Narasimhan, S. V.; Raj, B. *J. Nucl. Mater.* **2002**, *303*, 156.

(23) Yin, M.; Krupa, J. C.; Antic-Fidancev, E.; Lorriaux-Rubbens, A. *Phys. Rev. B* **2000**, *61*, 8073.

(24) Shishonok, E. M.; Philipp, A. R.; Shishonok, N. A.; Anichenko, N. G. *Phys. Status Solidi B* **2005**, *242*, 1700.

(25) Allieri, B.; Laura, E. D.; Alessandra, M.; Luigi, S.; Lucia, C.; Adolfo, S.; Marco, B. *Mater. Chem. Phys.* **2000**, *66*, 164.

(26) Wu, G. S.; Zhang, L. D.; Cheng, B. C.; Xie, T.; Yuan, X. Y. *J. Am. Chem. Soc.* **2004**, *126*, 5976.

(27) Xiao, Z. L.; Han, C. Y.; Welp, U.; Wang, H. H.; Kwok, W. K.; Willing, G. A.; Hiller, J. M.; Cook, R. E.; Miller, D. J.; Crabtree, G. W. *Nano Lett.* **2002**, *2*, 1293.

(28) Lakshmi, B. B.; Dorhout P. K.; Martin, C. R. *Chem. Mater.* **1997**, *9*, 857.

(29) Miao, Z.; Xu, D. S.; Ouyang, J. H.; Guo, G. L.; Zhao, X. S.; Tang, Y. Q. *Nano Lett.* **2002**, *2*, 717.

(30) (a) Zhou, Y. K.; Huang J.; Shen, C. M.; Li, H. L. *Mater. Sci. Eng., A* **2002**, *335*, 260. (b) Zhou Y. K.; Shen, C. M.; Huang J.; Li, H. L. *Mater. Sci. Eng., B* **2002**, *95*, 77. (c) Zhou Y. K.; Shen, C. M.; Li, H. L. *Solid State Ionics* **2002**, *146*, 81.

(31) (a) Ji, G. B.; Tang, S. L.; Xu, B. L.; Gu, B. X.; Du, Y. W. *Chem. Phys. Lett.* **2003**, *379*, 484. (b) Yang, Z.; Huang, Y.; Dong, B.; Li, H. L.; Shi, S. Q. *Appl. Phys. A: Mater. Sci. Process.* **2006**, *84*, 117. (c) Zhou, Y. K.; Li, H. L. *J. Mater. Chem.* **2002**, *12*, 681.

(32) (a) Chu, S. Z.; Wada, K.; Inoue, S.; Todoroki, S. I. *Chem. Mater.* **2002**, *14*, 266. (b) Li, X. H.; Liu, W. M.; Li, H. L. *Appl. Phys. A: Mater. Sci. Process.* **2005**, *80*, 317. (c) Xiong, S. X.; Wang, Q.; Xia, H. S. *Synth. Met.* **2004**, *146*, 37.

(33) Linares, R. C. *J. Opt. Soc. Am.* **1966**, *56*, 1700.

(34) Breysse, M.; Faure, L. *J. Lumin.* **1981**, *26*, 107.

(35) Hubert, S.; Thouvenot, P. *J. Alloys Compd.* **1992**, *180*, 193.